

This is an author-created, un-copyedited version of an article accepted for publication in Physics in Medicine and Biology. IOP Publishing Ltd is not responsible for any errors or omissions in this version of the manuscript or any version derived from it. The definitive publisher authenticated version is available online at <http://www.iop.org/EJ/abstract/0031-9155/50/13/007>.

**The Three Dimensional Scintillation Dosimetry Method:
Test for a ^{106}Ru eye plaque applicator**

Kirov AS^{1*}, Piao J Z², Mathur N K¹, Miller T R³, Devic S⁴,
Trichter S⁵, Zaider M¹, Soares CG⁶, and LoSasso T¹

¹Memorial Sloan-Kettering Cancer Center, New York, NY

²Case Western Reserve University, Cleveland, OH

³Mallinckrodt Institute of Radiology, Washington University, Saint Louis, MO

⁴Department of Medical Physics, McGill University, Montreal, Canada

⁵Radiation Oncology, New York Presbyterian Hospital, Weill Cornell Medical Center, New York, NY

⁶National Institute of Standards and Technology, Gaithersburg, MD

*Corresponding Author:

Assen S. Kirov

Department of Medical Physics

Memorial Sloan-Kettering Cancer Center

1275 York Avenue

New York, NY 10021

kirova@mskcc.org

The need for fast, accurate, and high resolution dosimetric quality assurance in radiation therapy has been outpacing the development of new and improved 2D and 3D dosimetry techniques. This paper summarizes the efforts to create a novel and potentially very fast, 3D dosimetry method based on the observation of scintillation light from an irradiated liquid scintillator volume serving simultaneously as a phantom material and as a dose detector medium. The method named Three Dimensional Scintillation Dosimetry (3DSD) uses visible light images of the liquid scintillator volume at multiple angles and applies a tomographic algorithm to a series of these images to reconstruct the scintillation light emission density in each voxel of the volume. It is based on the hypothesis that with careful design and data processing one can achieve acceptable proportionality between the local light emission density and the locally absorbed dose. The method is applied to a Ru-106 eye plaque immersed in a 16.4 cm³ liquid scintillator volume and the reconstructed 3D dose map is compared along selected profiles and planes with radiochromic film and diode measurements. The comparison indicates that the 3DSD method agrees, within 25% for most points or within ~ 2 mm distance to agreement, with the relative radiochromic film and diode dose distributions in a small (~ 4.5 mm high and ~ 12 mm diameter) volume in the unobstructed, high gradient dose region outside the edge of the plaque. For a comparison, the reproducibility of the radiochromic film results for our measurements ranges from 10 to 15% within this volume. At present, the 3DSD method is not accurate close to the edge of the plaque, and further than ~10 mm (<10% central axis depth dose) from the plaque surface. Improvement strategies, considered important to provide a more accurate quick check of the dose profiles in 3D for brachytherapy applicators are discussed.

1. Introduction.

A variety of 1D, 2D and 3D dose measurement techniques are currently available to the radiation therapy community. Ionization chambers, thermoluminescence dosimeters (TLD), diodes, and plastic scintillator probes provide accurate dose on a point by point basis (Seuntjens *et al* 2000, Duggan *et al* 2004, Kirov *et al* 1995, Onori *et al* 2000, Beddar A. S. *et al* 1992a, Beddar A. S. *et al* 1992b,c, Flühs D *et al* 1996, Williamson *et al* 1999). Radiochromic and radiographic films can measure the dose distribution in a plane, but they suffer from uniformity and energy dependence issues, respectively (Bohm *et al* 2001, Dempsey *et al* 1999, Devic S *et al* 2004, Danciu *et al* 2001, Palm *et al* 2004). Polymerizing and Fricke gels (Maryański *et al* 1996, Olsson *et al* 1998) provide realistic 3D dose distributions. Recently, electronic portal imaging devices (EPID)(Chang *et al* 2001, Turian *et al* 2004) have been used for dosimetry. Radiochromic films require lengthy data acquisition times and waiting periods prior to processing of the data to obtain the dose. The 2D and 3D techniques often require special phantom preparations in order to accommodate a brachytherapy applicator and to perform the measurements. In contrast, a volume filled with a liquid scintillating solution will provide immediately recordable signals and can easily accommodate an applicator of any shape.

The development of the Three Dimensional Scintillation Dosimetry (3DSD) technique (Kirov *et al* 2002b) is aimed at providing, in the long term, a practically real time 3D dose measurement method based on detecting the scintillation light signal from an irradiated volume. It is a 3D extension to previous work (Perera *et al* 1992, Williamson *et al* 1999, Kirov *et al* 1999a, Kirov *et al* 2000a) for developing a 2D dosimeter using a plastic scintillator sheet immersed in water. In the present method, relative 3D dosimetry is performed by applying tomographic reconstruction to optical luminescence produced by the source under investigation in a liquid scintillation volume. One of the most important applications of this method may be small brachytherapy applicators with asymmetrical shapes. Examples are eye plaques for treatment of ocular melanoma, which may vary in geometrical design, type of radiation, and source isotope used (Hungerford 2003, Chan *et al* 2001, Flühs D *et al* 2004). There is an increased demand to evaluate the dosimetric properties of this type of devices in a short time. The advantage of 3DSD for such cases comes from the potentially high measurement speed and the ease of accommodating applicators with arbitrary complex shapes. These features are difficult to achieve with either solid or gel phantom dosimetry techniques.

The development of the 3DSD method followed several steps described previously (Kirov *et al* 1999b, Kirov *et al* 2000c, Piao and Kirov 2001, Kirov 2001, Kirov *et al* 2002a, Kirov *et al* 2002b). Preliminary results for relative dosimetry around an ^{125}I seed obtained by detecting light only under a single angle indicated the potential of the method to provide relative 3D dose distributions if images of the scintillation volume under multiple angles are obtained. With respect to possible applications of the 3DSD method

to external beam megavoltage therapy applications, the contribution of Cerenkov radiation was measured and was estimated to be between 2 and 6% for 6 MV photons and between 3 and 10% for 18 MV photons(Kirov *et al* 2000b).

In this paper we use the 3DSD method to measure the dose distribution close to the ^{106}Ru CCX type eye plaque (Bebig Isotopen- und Medizintechnik GmbH, Berlin, Germany*), which has been under intensive quality assurance tests recently(Soares *et al* 2001, Trichter *et al* 2002, Kaulich *et al* 2004). Diode measurements for the same model eye plaque and radiochromic film (RCF) measurements for the same individual eye plaque (serial number 41) used in these 3DSD measurements are also presented for comparison to test the accuracy of the method in the unobstructed part of the volume.

2.Method

2.1. The liquid scintillator

The liquid scintillator in the cell plays the role of both a water equivalent phantom material and a dose measurement medium. The properties of various liquid scintillator solutions as a dosimeter were studied previously (Kirov *et al* 2000c) and it was shown that with appropriate additives (Poly(methylphenylsiloxane) (PMPS) or similar Si containing compounds) dosimetric water equivalence can be achieved in broad energy intervals while preserving high scintillation light output. In this work we use the M4 liquid scintillator mixture (Pseudocumene + 15 g/l $[\text{PFI}(\text{Pr})_2]_2$ (Exciton Corp.)) from this paper, loaded with 27.5 % PMPS, (Aldrich Chemical Co. Inc, Milwaukee, Wisconsin) by weight of the final solution. The liquid scintillator was bubbled with nitrogen gas after pouring into the cell to reduce oxygen content and the associated scintillation quenching. The point spread function of the liquid scintillator response to dose for a similar liquid scintillator, BC505, (Bicron Corporation, Newbury, Ohio) was previously determined to be represented well by a pseudo-Voigt function: a linear combination of Lorentzian and Gaussian functions (Kirov 2001). The liquid scintillator point spread function model consists of a sharp Gaussian peak (< 0.2 mm FWHM) superimposed on a broader (> 10 mm FWHM) and Lorentzian peak with ~ 100 times weaker peak amplitude. Light attenuation within the experimental cell was determined to be negligible for the few cm light path through the liquid scintillator solution (Kirov *et al* 2002a).

2.2. Measurement setup

A photograph and a schematic of the experimental arrangement are shown in figure 1. The setup used in this work differs from the one described previously(Kirov *et al* 2002b), by the addition of an angular stage which allows accurate selection of the source rotation angle with respect to the device optical axis determined by the collimator grid. The liquid scintillator is held in a square cross-section vessel (cell) with inner sides of 25.4 mm. The cell is manufactured from black plastic (Delrin) and sand blasted to further decrease

* In this paper certain commercially available products are identified by name. These identifications are made for informational purposes only and do not imply endorsement by any of the authors or by their institutions, nor do they imply that these are the best or only products available for the purposes described.

light reflection from the cell walls. Although the cell could in principle be accommodated in a larger water phantom, we consider this to be an unnecessary complication of the measurement geometry for the ^{106}Ru beta source: the backscatter of the small number of photons (~ 0.34 per decay) following the β -decay back into the measurement volume from a larger phantom would be a negligible addition to the electron dose.

The CCX eye plaque is attached using one suture tab hole to a vertical cylindrical holder aligned with the central axis of the cell (figure 2). The center of the inner surface of the eye plaque is 1.4 mm below the top of the measurement volume defined by the size of the square window of the cell. To decrease edge artifacts (see end of §2.4), the size of the reconstruction volume is selected to be slightly larger than the cell (27.1488 mm sides). This volume is divided into $64 \times 64 \times 64$ cubic voxels with 0.4242 mm sides defining the measurement slice thickness. The centers of the first horizontal slice below the rim of the plaque and of the first slice below the plaque suture tabs are at 1.57 mm and at 3.27 mm from the center of the inner surface of the plaque, respectively. The scintillation light passes through an optical window and a collimator grid and is reflected by a mirror to reach the CCD camera, a liquid nitrogen cooled very low noise camera supplied with a high grade (no bad pixels), back illuminated UV enhanced sensor divided into 512×512 pixels (Princeton Instruments, Roper Scientific, Trenton, NJ). The grid (20 μm diameter holes packed hexagonally in 2 mm thick black glass, Collimated Holes, Inc., Campbell, CA) transmits light photons emitted from the measurement volume in a direction perpendicular to the cell window. To the CCD camera we attached a high transmittance, low distortion, multi-component lens (Schneider Optische Werke GmbH, Bad Kreuznach, Germany) positioned at optical path distance of 34.5 cm, which is focused on the back surface (towards CCD camera) of the collimator grid. The distance from the front surface of the collimator grid to the front surface of the measurement cell window is 11 cm. Placing the grid outside the cell takes advantage of the differences in refraction indices between the liquid scintillator, the glass of the cell window, and air to increase the collimating power of the grid since photons not parallel to the optical axis will be refracted at larger angles when exiting the cell. The mirror and lead bricks are used to shield the camera from direct interactions of x-rays and gamma-rays with the detector chip. The liquid scintillator phantom, collimator grid, mirror, and camera are aligned and mounted on two perpendicular optical rails, which allow smooth variation of the distance between the components. The source holder can be rotated around the vertical axis, which allows the collection of data at different angles. The optical rails are attached to a platform rigidly bolted to a heavy-duty cart placed in a dark room and covered with a thick black felt sheet during measurements.

2.3. Measurements

Images of the scintillating volume are acquired for 64 different orientations of the plaque with respect to the system's optical axis $360/64=5.625^\circ$ apart. The angle selection is performed manually with accuracy of $\sim 0.1^\circ$. At each angle five 1-minute exposures are accumulated using the automatic mode of the WinSpec software (Princeton Instruments, Roper Scientific, Trenton, NJ). To estimate the dark image counts, 20 exposures of one

minute each are accumulated for each of the following three conditions: i) shutter of the CCD camera open, and source removed from the liquid scintillator cell; ii) shutter closed, source left inside the liquid scintillator cell; iii) shutter closed, source removed.

2.4. Data analysis

Part of the images containing 448 x 448 pixels and corresponding to the 27.15 x 27.15 mm square on the collimator grid surface is selected and further analyzed in the following way. The five images at each of the 64 angles are inspected and defective images (e.g. due to excessive accidental ambient light) are discarded. Then the mean and the standard deviation for each pixel value are determined at each angle. In almost all images a few pixels are observed having very high values, or “spikes”, due to direct interaction of scattered photons or cosmic rays in the CCD chip. Rejection of these spikes is performed by assuming a Poisson distribution of the pixel counts around the mean pixel values. At each pixel, we calculate the mean and standard deviation. If the observed standard deviation differs by more than $3\sqrt{mean}$, the pixel is identified as contaminated. For such a pixel we assume that at least one of the N (=5) pixel intensity values associated with this pixel is a spike. The five values for each pixel are sorted in order of increasing value and the maximum value is rejected. The same procedure is performed over the remaining (N-1) values. The rejected values are replaced by the mean pixel value of the remaining frames (Devic S *et al* 1999). Less than a percent of the pixels are affected by this procedure. After spike removal the mean images are corrected for dark image counts estimated from the three dark measurement sets indicated in 2.3 using the formula $D = D_1 + (D_2 - D_3)$, where, D_1 , D_2 , and D_3 are the mean of 20 spike rejected images obtained, respectively with: shutter open and source removed, shutter closed and source in, and shutter closed and source removed. For the mean pixel values we obtain $D_1 = 177.2$, $D_2 - D_3 = 1.3$, and $D = 178.5$ counts. The fraction of the dark counts due to the presence of the source, $(D_2 - D_3)$, is reduced by the spike rejection procedure and is relatively small, nevertheless, it is significant for the darker part of the images.

A so-called “chicken wire” artifact, caused by the shadow of the hexagonal hole structure of the collimator grid is observed in the mean net images. The net images are smoothed to reduce this artifact. Smoothing in the vertical direction creates vertical lines with lower intensity in the resulting images, due to vertical alignment of the hexagon edge shadows. Therefore we apply smoothing of the mean images in the horizontal direction only. Each horizontal profile is smoothed by piece-wise cubic-spline fit over every 20 points (~ 1.2 mm) of the profile. After smoothing, the 64 images are compressed (7:1) into smaller matrices with 0.4242 mm pixel size and containing 64 x 64 pixels each (figure 3). In this way the images passed to the reconstruction algorithm are slightly larger (27.15 mm square) than the window size (25.4 mm square). This is done to push the edge artifacts of the MLEM reconstruction (Snyder *et al* 1987) away from the edge of the measurement volume. Finally the 64 images are combined into a single file, which is readable by the image reconstruction program.

2.5. Optical Tomographic Reconstruction

To reconstruct the 3D scintillation light emission density we use a SPECT Maximum Likelihood Expectation Maximization (MLEM) algorithm (Wallis and Miller 1993). The algorithm is modified to incorporate a 3D aperture function. The Ordered Subset Expectation Maximization (OSEM) option of the MLEM reconstruction algorithm is used with 8 subsets and a number of iterations varying from 5 to 40. To enhance convergence, the Median Root Prior (MRP) filter (Alenius and Ruotsalainen 1997) is implemented (Piao and Kirov 2001). The restriction imposed on each pixel's value is determined from a prior Gaussian distribution, centered at the median of a predefined neighborhood of the pixel (Alenius and Ruotsalainen 1997, Alenius *et al* 1998). This regularization is based on the assumption of local monotonic behavior of the emission density, which is valid for dosimetry applications. The One Step Late (OSL) MRP algorithm is presented by:

$$\lambda_b^{(k+1)} = \frac{\lambda_b^{(k+1)MLEM}}{1 + \beta \frac{\lambda_b^{(k)} - M}{M}} \quad (1)$$

Here, $\lambda_b^{(k+1)MLEM}$ is the (k+1)-th estimate of the emission density in pixel b before MRP penalization, $\lambda_b^{(k)}$ and $\lambda_b^{(k+1)}$ are the k-th and (k+1)-th estimates of the emission density in pixel b after the MRP penalization, $M = Med(\lambda^{(k)}, b)$ is the median pixel value in a small neighborhood around pixel b , and $0 < \beta \leq 1$ is the weight of the restriction. MRP penalization with $\beta=0.3$ for a cubic volume region with side of 5 pixels (~ 2 mm) is used.

The aperture diameter of the collimator grid as a function of depth is approximated by the relation $2.69 + 0.009375 n_z$ in pixels, where 2.69 pixels is the projection of the 20 micron diameter of the collimator grid hole, when viewed from the other side of the grid, at the center of the first vertical slice inside the cell, and n_z is the number of the vertical slice counting from the cell window. Tests are performed of the sensitivity of the results on the width of the aperture function, the weight of the MRP filter and on the iteration number. Typical reconstruction times are approximately 2 minutes per iteration on a 2.4 GHz computer, which, however, increases if the aperture function width or depth dependence coefficient deviated from the geometrical estimates of 2.69 pixels and 0.009375 pixels/pixel depth dependence given above.

2.6. Scintillator point spread function and other artifact corrections

The point spread function was measured in a 1 mm thin optical cell with light scattering conditions different from these in the current measurement cell (Kirov 2001, Kirov *et al* 2000a). To account for small, but nevertheless possible, light scatter from the roughened black Delrin cell walls, an estimate of the light scatter signal is made and subtracted from the reconstructed emission density. Further more, the edge artifacts cause a rise in the emission density close to the rim of the reconstruction volume. For this reason the emission density reaches a minimum value at ~ 4 -5 pixels from both ends in horizontal and vertical profiles through the center of the slice (dotted lines in Fig.6). For each slice the scattered light signal is assumed to be uniform and is approximated by the minimum

pixel value from these central profiles. In order to correct also for the edge artifacts, a correction 2D map is prepared for each slice, which has the peripheral rows and columns beyond the minimum emission density identical to those in the uncorrected slice and has the above constant value for all other points. These correction maps were subtracted from the corresponding emission density for each slice to produce scattered light and edge artifact corrected emission density.

To correct for the liquid scintillator point spread function, an iterative three-dimensional deconvolution program is developed by replacing the projection kernel in the MLEM algorithm (Wallis and Miller 1993) by the point spread function of the liquid scintillator. The 3D emission density in the volume can be presented by the 3D convolution: $I(\mathbf{u}) = \int P(\mathbf{u} | \mathbf{x}) \otimes \lambda(\mathbf{x})$, where \mathbf{x} and \mathbf{u} are three-dimensional coordinates in the measurement space, $P(\mathbf{u} | \mathbf{x})$ is the point spread function value for distance $|\mathbf{x}-\mathbf{u}|$, and $\lambda(\mathbf{x})$ is the object emission density to be retrieved. The non-negativity of the emission density and the point spread function allows us to use Csiszar's I-divergence as a discrepancy measure as in MLEM. Then, the update of the desired dose distribution after each iteration step is given by:

$$\lambda^{k+1}(\mathbf{x}) = \lambda^k(\mathbf{x}) \frac{1}{\sum_{\mathbf{u}} P(\mathbf{u} | \mathbf{x})} \sum_{\mathbf{u}} \left[\frac{P(\mathbf{u} | \mathbf{x})}{\sum_{\mathbf{x}'} P(\mathbf{u} | \mathbf{x}') \lambda^k(\mathbf{x}')} \right] I(\mathbf{u}), \quad (2)$$

where $\lambda^{k+1}(\mathbf{x})$ is the update at $k+1$ iterations. The scattered light and edge artifact corrected emission density is deconvolved using this 3D procedure in 2 iterations for the point spread function of the liquid scintillator response (Kirov 2001) to give the relative dose rate. MRP regularization (1) is implemented in the deconvolution process and is used with $\beta=0.3$ for a cube volume with side 5 pixels. The pixels in the corrected emission density for which division by zero occurs due to (1) are set to zero.

2.7. Radiochromic film and diode measurements

The 3DSD measurements are compared against radiochromic (RCF) film measurements of the same plaque (^{106}Ru , CCX 41, Bebig) performed at two different institutions (NIST and MSKCC) and against diode measurements of the same CCX type of plaque produced more recently (CCX 104). The radiochromic film measurements are made in a solid water phantom by using the MD-55-2 type of film at MSKCC and the HD-810 type of film at NIST following procedures described elsewhere (Soares *et al* 2001, Trichter *et al* 2002). At MSKCC the film irradiations took between 5 and 65 hours for each film and the films received doses of at least 30 Gy on the central axis. The films were scanned 48 hours after the end of the irradiation. All measurements for the CCX41 plaque were done within one year, first the NIST, then the MSKCC radiochromic film measurements over a period of 3 months, and then the 3DSD measurements at MSKCC in one day immediately after. Therefore the strength of the source during the 3DSD measurements was within $\sim 17\%$ of the source strength during the MSKCC radiochromic film measurements.

The diode measurements are performed with a 0.5 mm diameter stereotactic diode (SFD, Scanditronix Medical AB, Uppsala, Sweden) moved in directions along and perpendicular to the central axis with the help of a mechanical stage in a water phantom. The diode current is integrated over 30 s periods with a precise electrometer resulting in charges varying from 0.1 to ~150 pC.

3. Results

This section presents a comparison of the 3DSD results with the radiochromic film and diode measurements. The 3DSD method has the ambitious goal of providing simultaneously the relative dose distribution throughout a volume. However, in addition to the 3DSD method, inaccuracies exist in the data used for validation as well as in the registration between the different data sets. Therefore, for better illustration and understanding of the differences, the comparison is performed separately along the eye plaque central axis and within slices at different distances from the plaque. An assessment of the accuracy over the volume is presented at the end of the discussion section.

The relative dose and the emission density distribution along the vertical axis through the center of the source and the liquid scintillator volume is shown in figure 4. The emission density data is averaged across a 2×2 pixel ($= 0.72 \text{ mm}^2$ square) cross section area column near the axis of the plaque to approximate the 1 mm^2 pixel size from the radiochromic film measurements presented by symbols. The dotted and dashed curves correspond to emission density obtained with different number of reconstruction iterations, 5 and 40 respectively. The solid curve represents the relative dose obtained after light scatter and edge artifact correction and deconvolution (2 iterations) of the liquid scintillator point spread function from the emission density obtained after a 10-iteration reconstruction. The 3DSD curves and the radiochromic film data are normalized at 5.4 mm from the inner plaque surface by setting the NIST value to match the equalized 3DSD values at this point. The ratio between the NIST and MSKCC data was preserved. The diode data at 5.74 mm was also normalized at the same point. No radiochromic film data is available for comparison further than 7.5 mm away from the inner surface of the plaque.

As seen in figure 4, increasing the number of iterations in the reconstruction leads to an increase of the slope and of what appears to be noise at some parts of the image: i.e. around 13 mm from the inner surface. However, the slope converged at about 10 iterations (not shown) and increasing the number of iterations up to 40 did not lead to significant changes in the central axis profile. Increasing the width of the aperture function used in the reconstruction above the selected value of 2.69 pixels additionally increases the dose fall off gradient on the central axis. Applying light scatter and edge artifact correction and liquid scintillator point spread function deconvolution also increased this gradient and resulted in closer agreement with the experimental points for the reconstruction, correction and deconvolution parameters selected (§2.5 and 2.6).

In figures 5 a-d and 6 a-d the emission density and the relative dose profiles obtained from the 3DSD method are compared to 2D distributions obtained by radiochromic film in 4 planes perpendicular to the plaque central axis. The absolute dose-rate levels quoted in these figures correspond to the start date of the MSKCC radiochromic film measurements.

In figure 5 the radiochromic film 2D dose distributions obtained at distances of 4.5, 5.4, 6.4, and 7.4 mm from the inner plaque surface are plotted together with 3DSD data from the corresponding slices (#13, 15, 17 and 20 from the top) in the imaged volume. The depth of the radiochromic film measurements is matched to the nearest of the 3DSD slices, which occur at 0.4242 mm intervals. The 3DSD dose maps were normalized to the peak dose of the radiochromic film measurement, since the depth-dose agreement along the central axis was addressed in figure 4. This eliminates differences coming from the vertical alignment inaccuracy, as well as larger error due to radiochromic film dose level uncertainty (see RCF MSK-NIST differences in figure 4). For the comparison we selected 3DSD results obtained with the following parameters: i) emission density obtained by OSEM reconstruction with 10 iterations and MRP filter ($\beta=0.3$, $r_{MRP}=2.5$ pixels); and ii) the relative dose profile obtained from the emission density with light scatter and edge artifact correction, and with liquid scintillator point spread function deconvolution in 2 iterations with MRP filter ($\beta=0.3$, $r_{MRP}=2.5$ pixels).

The plaque suture tabs are at about 86° (~3 o'clock) and 176° (~12 o'clock) with respect to the optical axis (which is parallel to the y axes in figure 5) of the system. The central point of each slice is aligned to the center of the radiochromic film dose map determined from the fiducial markers on the film. A search for arbitrary shifts of the radiochromic film dose maps is performed to find better visual registration of the dose distributions in each slice. This results in small shifts with respect to the geometrical {liquid scintillator volume} to {RCF} alignment: the radiochromic film dose maps are shifted by -0.7 mm and by -0.5 mm along y for the slices at 4.5 mm and 5.4 mm (figure 5.a and 5.b), by 0.7 mm along x for the slice at 6.4 mm (figure 5.c), and not shifted for the slice at 7.4 mm (figure 5.d). The comparisons shown in figures 5 and 6 incorporate these shifts.

In figure 6 are shown relative dose profiles passing through the centers of reconstructed slices at distances from the plaque inner surface marked in the upper right corners. The profiles shown in the left part of the figure are vertical, while these on the right are horizontal, through the slices oriented as in figure 5. In Fig 6.a-d the 3DSD results are compared to both radiochromic film profiles from the distributions shown in figure 5 and to diode measured profiles. Both the 3DSD emission density and relative dose-rate profiles are normalized at the peak point of the MSKCC radiochromic film data for each slice to better compare the shape of the dose distribution within the slice. The normalization factors used for the slices at 5.4, 6.4 and 7.4 mm are 0.1587, 0.1245 and 0.1198 respectively for the 3DSD uncorrected emission density, and 0.1667, 0.1454, and 0.1616 for the relative dose obtained after light scatter and edge artifact correction and liquid scintillator point spread function deconvolution. The maximum variation of the normalization factor is 29 % before and 13 % after the corrections and deconvolution. The latter number is comparable to the measurement uncertainty seen between the two

radiochromic film data sets. Note that in figure 4. the NIST and MSKCC radiochromic film data points differ by about 15 %, 10 % and 10 % at 5.4, 6.4 and 7.4 mm distances respectively.

In figure 6 e-f is shown comparison of profiles at distances 8.5 and 10 mm from the inner surface of the plaque as obtained by the 3DSD method and diode measurements only since no radiochromic film data is available at these distances. The 3DSD profiles are normalized with the factor (0.1616) obtained from the slice at 7.4 mm. The diode data is normalized to the 3DSD relative dose rate profiles at the highest point.

Smoothing of the images to eliminate the grid (“chicken wire”) artifact had practically no effect on the reconstructed emission density presented.

4. Discussion

4.1. Central Axis Depth dose curve

In the current arrangement the 3DSD method is not useful for the volume between the inner surface of the plaque and the distal edge of the plaque suture tabs (from 0 to 3.3 mm) since the opaque plaque blocks the scintillation light. For the region between the rim and the end of the plaque suture tabs (1.4 to 3.3 mm), accuracy could be improved if the presence of partially blocked projections is accounted for in the reconstruction. For the region between the inner plaque surface and the rim (0 to 1.4 mm), a 3DSD measurement is, in principle, possible if in addition to accounting for the blocked projections, the experimental arrangement, is modified to allow images of the plaque inner surface from different angles, and the plaque surface is covered with antireflective coating.

In Figure 4 agreement with the slope of the radiochromic film and diode measurements is observed from 5.4 mm to ~ 10 mm from the inner surface of the plaque. In the first 2 mm beyond the suture tabs (3.3 to 5.4 mm from the surface) the reconstructed emission density does not match the steep central axis dose profile as measured by radiochromic film and the diode. Turning on and off the MRP regularization filter during the reconstruction step showed that this rounding close to the rim is not due to the use of MRP filtering. The inaccuracy of the 3DSD method in this region may be related to a combination of factors discussed in detail in §4.4 in addition to the uncertainty in the plaque position and axial orientation. As possible sources for the over-estimation of the relative dose beyond 10 mm from the plaque surface, the reader is also pointed to the factors and approximations listed in §4.4.

4.2. Transaxial slices

In figures 5a-d the 3DSD relative dose-rates (dashed lines) are obtained from the emission densities (dotted lines) by light scatter and edge artifact correction and 3D liquid scintillator point spread function deconvolution (2 iterations). The overlay with the dose-rate as measured by radiochromic film (solid lines) shows a good overall agreement for all four slices. Near the plaque rim and suture tabs (the slice at 4.5 mm) the shape of the dose distribution for 3DSD relative to film is consistent (figure 5.a, and 6.a), although the absolute peak dose is substantially lower (figure 4).

Lateral shifts in different direction (≤ 0.7 mm, see §3), were needed for optimal registration with respect to the direct geometrical alignment between the measurement volume and the radiochromic film central axis point. These shifts may be indicative of the positional uncertainty of the measurements, or on the other hand could be due to the sensitivity of the MLEM reconstruction algorithm to noise. The small magnitude of these lateral shifts together with the depth dose comparison in figure 4, points to good relative agreement of the volumetric dose distribution obtained with the two methods between 5.4 and 7.5 mm from the plaque surface.

Quantifying the discrepancies between the 3DSD and the radiochromic film measurements by calculating ratios of the relative dose profiles from figure 6 showed that the agreement is within $\sim 25\%$ for most points of the central 12 mm diameter region along the vertical profiles and can reach 40% for some (close to horizontal) profiles for the same region. The maximum distance between the corresponding isodose lines is ~ 1.5 mm for the 90 cGy/h isodose-rate contour for the slice at 5.4 mm and is less than ~ 1 mm for the other slices. The 3DSD dose distribution is slightly narrower than the radiochromic film for figure 5 a-c, but matches better the radiochromic film profile dose-rate at 7.4 mm. Figures 6.e and f show that at 8.5 mm from the plaque the 3DSD and diode profiles agree within $\sim 20\%$ at up to more than 7.5 mm from the central axis and within ~ 2 mm distance to agreement up to 10 mm off axis for both slices at 8.5 and 10 cm distance.

The dose contours from the radiochromic film exhibit noticeable asymmetry and elongation along a horizontal direction (close to the 9 o'clock - 3 o'clock line in the figures) as well as extension towards 12 o'clock of the outer contours in the 4.5 to 6.4 mm slices. The plaque suture tabs are at ~ 12 o'clock and ~ 3 o'clock and it is not clear if the deviation from symmetry in the radiochromic film data corresponds to additional activity at the suture tabs, or due to an artifact of the film. The 3DSD contours are more symmetric, but the suture tab extensions are blocking scintillation light, which could suppress the effect of higher dose at these locations. The non-uniformity of the MD-55-2 film response (Niroomand-Rad *et al* 2005), which is not corrected for in these measurements, could cause isodose contour elongation in one direction. At the same time, for the points within 5 mm from the plaque central axis in the slices at 4.5, 5.4 and 6.4 mm, the diode profiles, also measured along lines passing above one of the plaque suture tabs, are broader than the 3DSD profiles and agree better with the radiochromic film profiles. However, since the diode measurements were performed for a different plaque and only in one direction, no conclusions about the asymmetry of the contours can be drawn.

At off axis distances larger than the plaque radius (5.8 mm) the 3DSD measured dose-rates agree with the diode points up to 10 mm off axis, while the radiochromic film results are higher for all four slices. It is unlikely that the decrease of response for lateral irradiation for our diode ($\sim 7\%$ at 90° from the normal to the front surface observed in a ^{60}Co beam) is causing significant loss of efficiency, since most of the dose for all diode points from the off-axis profiles at 5.5 to 10 mm axial distances would be coming from the front of the diode. The radiochromic film could overestimate dose in these regions due to dose dependent optical density growth.

4.3. Volumetric comparison

In the previous sections we discuss separately the evaluation of the 3DSD method along the plaque central axis and in transaxial slices. If the MSKCC radiochromic film and the volumetric 3DSD dose distributions are normalized at a single point, the highest point at 5.4 mm, a similar overall agreement for the same volume is obtained: within $\sim 25\%$ for most points and up to 45% or ~ 2 mm maximum distance to agreement for a volume ~ 12 mm in diameter and ~ 4.5 mm high (between 5.4 and 10 mm from the plaque surface). For such normalization the disagreement is greatest near the central axis but improves away from the axis due to a compensation effect: the 3DSD points from figure 6 are moved up for the slices further away due to the larger normalization factor. The 3DSD relative dose agrees with the plaque axis depth dose curve from the NIST radiochromic film measurement. Therefore such renormalization with depth, when a single normalization point is taken, would not occur if the MSKCC agreed better with the NIST radiochromic film axial measurements.

The achieved relative accuracy of $\sim 25\%$ by the 3DSD method for most points in the indicated volume is larger, but still comparable to the reproducibility of the radiochromic film results, $\sim 15\%$. This radiochromic film uncertainty is also comparable to but slightly larger than, the agreement margin (10-14% absolute, 3-9% relative) between the various 1D and 2D methods compared for a different ^{106}Ru plaque in a previous work (Soares *et al* 2001).

4.4. Possible sources for the observed discrepancies

The following is a list of possible sources of inaccuracy in the current realization of the 3DSD method:

- 1) Despite the special precautions in the cell manufacturing (sand blasted black Delrin walls) light scattered in the cell can still contribute to the emission density. This is not fully accounted for by the liquid scintillator point spread function, obtained for a different cell design and a similar scintillator solution (§2.1). In this work, the scattered light signal in the portion of the reconstructed slices, not affected by the MLEM edge artifacts was approximated by a constant as described in §2.6, which may not be sufficiently accurate. Subtraction of an estimate of the scattered light was attempted also prior to MLEM reconstruction by subtracting a constant image, matching the light signal

level 4 pixels from the lateral edges, for each of the 64 images. This resulted in zeroing the 4 left most and right most pixel columns in each image, which in the subsequent MLEM reconstruction produces a MLEM edge artifact closer to the central axis: a ring with increased emission density at ~ 9 mm radius. For this reason, this second approach to light scatter correction was abandoned.

2) In the reconstruction algorithm an approximation was used for the collimator aperture function and the contribution of the other optical components (cell window, collimator grid and mirror) to the overall optical system resolution was not accounted for. This may contribute to the dose discrepancy close to the plaque.

3) Uncertainty close to the volume boundaries is introduced by the square cross section of the cell volume, which results in missing projections for some angles for part of the dose distribution, in the regions of the volume between the cell walls and an inscribed vertical cylinder. There is also a difference in handling the projections between the experiment on one hand and the reconstruction algorithm. In the experiment the detected light rays are always perpendicular to one side of the cubic measurement volume. The MLEM algorithm, however, which uses as an initial approximation, a cube with emission density of 1 for all voxels, “sees” the entire non-zero emission density volume under all angles, i.e. the forward projections of the volume are not always perpendicular to one side of the cube. The measurement geometry selected in this work, which uses a cell with square cross section, is a tradeoff for the minimal distortion and better projection collimation.

4) Scintillation quenching (Birks J B 1964, Williamson *et al* 1999) due to increase of the ionization density at low electron energies, less than ~ 100 keV, (Horrocks D L 1964, Peron M N and Cassette P 1996) has not been studied for this scintillator and electron source. Energy dependent scintillation quenching is expected to affect accuracy at the end, the last ~ 0.5 mm, of the electron tracks, where the electron energy falls in that range.

5) For ^{106}Ru sources Cerenkov light contributes to the detected light due to the sufficiently energetic beta spectrum: 3.541 MeV maximum and ~ 1.4 MeV average beta energy. At 90° with respect to a 6 MV photon beam (similar average energy of the secondary electrons), Cerenkov radiation was shown (Kirov *et al* 2000b) to contribute between 2 and 6 % of the signal. Therefore, Cerenkov contribution to the detected light of a few percent, that will decrease with decreasing electron energy away from the plaque is reasonable. Beyond the electron range (~ 7 mm for the average and ~ 18 mm for the maximum energy electrons), Cerenkov light can be produced only by electrons set in motion either by the Rh-106 gamma rays (~ 0.34 per decay) or by bremsstrahlung x-rays produced by the electrons (< 5 % of the energy loss), and is expected to be less than $\sim 1\%$.

As indicated in §3 the obtained agreement is dependent on the selection of the reconstruction, light scatter correction and deconvolution parameters. Therefore careful selection and validation of these parameters will need to be performed if the method is tested for a different experimental arrangement. While the parameters selected in this work reflect our current best estimates, changes are possible in the future for a modified cell and optical system design.

Finally, a part of the observed discrepancies with radiochromic film measurements could be due to the limited accuracy of the radiochromic film results. Uncertainties of $\sim 7.5\%$ (1σ) were previously reported for a similar ^{106}Ru plaque (Soares *et al* 2001). The accuracy of the radiochromic film results could be related to the film non-uniform sensitivity, to the dependence on dose of the radiochromic film optical density growth with time (Ali *et al* 2003, Ali *et al* 2005), to unaccounted for film scanner point spread function effect in the high gradient regions (Dempsey *et al* 1999), and to the increased radiochromic film measurement uncertainties at low doses.

4.5 For further development

The spatial resolution of the method is a combination of the effects of the voxel size (0.4242 mm), the width of the liquid scintillator point spread function (see §2.1), the width of the collimator aperture function (§2), and the influence of the reconstruction algorithm and the other optical components. To determine the overall resolution of the optical system, the design of a separate measurement with a very small (approximating a point) source, or a sharp edge or thin slit of light in the place of the measurement cell is needed. The point spread function of the optical system obtained in this way, will need to be convolved with the liquid scintillator point spread function as determined at different positions within the measurement cell to include the effect of the cell specific light scatter. Such investigation is beyond the scope of the present study and suggested for future work.

In order to obtain accurate results with the 3DSD method over larger volumes, further research in the following directions is suggested: i) closer matching of the density of the liquid scintillator to water (1 g/cm^3) compared to the current $\sim 0.93 \text{ g/cm}^3$; ii) re-assessment of the shape of the point spread function inside the actual 3DSD measurement cell for the liquid scintillator mixture intended for dosimetry; iii) determination of the energy- and dose-rate- dependence of the scintillation light output; iv) measurement of the light scatter within the 3DSD measurement cell volume as well as of artifacts from the other optical bench components: cell window, collimator grid, mirror and lens; v) enhancement of the method to perform 3D dose measurements in a region for which part of the projections are blocked. One way to reduce the artifacts that will arise from the presence of such incomplete projections in the volume, is to give to the reconstruction algorithm the exact position and shape of the opaque objects, so that a correct length of the light integration path is used. Based on this principle, approximate measurements even around concave portions of an applicator (i.e. inside the plaque) could be possible by collecting luminescence at angles from which the concave portion of the applicator is seen, and light reflection from the applicator surface is prevented.

Application of the 3DSD method for larger volumes required by other applications like Intensity Modulated Radiation Therapy (IMRT) or proton dosimetry will require yet further investigations. For liquid scintillator volumes larger than few centimeters light attenuation due to self absorption in the liquid scintillator will need to be accounted for. In the cases of IMRT, Dynamic Wedge, and Robotic Radiosurgery treatments, the radiation intensity pattern changes with time, and performing the measurements with a

single detector system may take a prohibitively long time. To avoid repeating the treatment sequence for every measurement angle, a multiple detector system may have to be developed. At the same time, the 3DSD measurement cell needs to be designed in such a way that it causes only minimal or controllable image distortions. In the case of a cylindrical or spherical measurement volume there will be image aberrations due to refraction at the interfaces between the vessel walls, the liquid scintillator and air. A measurement cell with a few flat windows and light detectors looking at a cubic volume under two or another small number of directions may turn out to be a good compromise. Such a configuration may find application, for example, for fast evaluation of the dose distribution close to symmetrical heterogeneities inserted in the liquid scintillator volume without full 3D reconstruction. Applications to proton or heavy ion dosimetry will require careful characterization of LET dependence of the liquid scintillator response similar to studies performed for polymer gels (Gustavsson *et al* 2004).

5. Conclusions

This paper evaluates the accuracy and potential of a new relative 3D dose measurement method (3DSD) in which a liquid scintillator volume is used simultaneously as a water equivalent phantom material and as a dose measurement medium. In the paper is tested the ability of optical tomography to achieve sufficiently high quantitative 3D accuracy from reconstruction of 2D emission images, so that it can serve to radiation dosimetry.

The 3DSD method applied to a CCX ^{106}Ru plaque provided a relative dose distribution which agreed with radiochromic film and diode data within 25 % for most points and within less than 45 % or 2 mm distance to agreement for all points in a cylindrical volume about 4.5 mm high and ~ 12 mm in diameter, starting ~ 2 mm away from the plaque suture tabs. For a comparison the spread of the radiochromic film measurements ranges from 10 to 15% for these distances. The currently observed inaccuracies are expected to be primarily due to the approximations used for the overall system and liquid scintillator point spread functions, to the approximate light scatter correction, to distortions by the reconstruction algorithm and to other factors listed in the discussion. It should be emphasized that applying light scatter correction and liquid scintillator point spread function deconvolution to the reconstructed emission density was needed to correctly deduce the central axis relative dose distribution, and that the subtraction of an approximation of the edge artifacts improved agreement close to the cell walls. The results are dependent on the reconstruction, correction and deconvolution parameters selected.

The 3DSD method has the potential to provide relative dose distributions in a small volume away from the obstructed part of the volume, with accuracy and resolution that could be comparable to the existent experimental techniques for small and complex shaped brachytherapy applicators. Since the measurement and dose reconstruction procedure can be made fully automatic, the method provides prospects for performing fast and labor efficient checks of the dose shape in 3D for such applicators.

Acknowledgments

This work was supported in part by grants from the Whitaker Foundation (No. 97-0336) and from Washington University in Saint Louis. The authors are grateful to Dr. Walter Robert Binns and to John Epstein from the Department of Physics at Washington University in Saint Louis, and to Ricardo Jovantes, MSKCC, for their help in the design of the experimental cell and of the experimental arrangement and to Dr. Donald Snyder from the Department of Electrical Engineering at Washington University in Saint Louis for helpful discussions. One of us (ASK) would like to acknowledge also the support for this project from Dr. Jeffrey Williamson, Virginia Commonwealth University, from Dr. Timothy Kinsella, Ireland Cancer Center, University Hospitals of Cleveland, and from Dr. Claudio Sibata, East Carolina University School of Medicine, and to dedicate his contribution to this work to the memory of his parents.

References

- Alenius S and Ruotsalainen U 1997 Bayesian image reconstruction for emission tomography based on median root prior *Eur. J. Nucl. Med.* **24** 258-265
- Alenius S, Ruotsalainen U, and Astola J 1998 Using local median as the location of the prior distribution in iterative emission tomography image reconstruction *IEEE Trans. on Nucl. Sc.* **45** 3097-3104
- Ali I, Costescu C, Vicic M, Dempsey J F, and Williamson J F 2003 Dependence of radiochromic film optical density post-exposure kinetics on dose and dose fractionation *Med Phys* **30** 1958-67
- Ali I, Williamson J F, Costescu C, and Dempsey J F 2005 Dependence of radiochromic film response kinetics on fractionated doses *Appl Radiat Isot* **62** 609-17
- Beddar A S, Mackie T R, and Attix F H 1992a Cerenkov light generated in optical fibers and other light pipes irradiated by electron beams *Phys. Med. Biol.* **37** 925-35
- Beddar A S, Mackie T R, and Attix F H 1992b Water-equivalent plastic scintillation detectors for high-energy beam dosimetry: II. Properties and measurements *Phys. Med. Biol.* **37** 1901-13
- Beddar A S, Mackie T R, and Attix F H 1992c Water-equivalent plastic scintillation detectors for high-energy beam dosimetry: I. Physical characteristics and theoretical consideration *Phys. Med. Biol.* **37** 1883-900
- Birks J B 1964 *The theory and practice of scintillation counting*, (New York:Pergamon)
- Bohm T D, Pearson D W, and Das R K 2001 Measurements and Monte Carlo calculations to determine the absolute detector response of radiochromic film for brachytherapy dosimetry *Med. Phys.* **28** 142-146

Chan M, Fung AY, Hu YC, Chui CS, Amols H, Zaider M, and Abramson D 2001 The measurement of three dimensional dose distribution of a ruthenium-106 ophthalmological applicator using magnetic resonance imaging of BANG polymer gels *J. Appl. Clin. Med. Phys.* **2** 85-9

Chang J, Mageras G S, Ling C C, and Lutz W 2001 An iterative EPID calibration procedure for dosimetric verification that considers the EPID scattering factor *Med. Phys.* **28** 2247-2257

Danciu C, Proimos B S, Rosenwald J C, and Mijnheer B J 2001 Variation of sensitometric curves of radiographic films in high energy photon beams *Med Phys* **28** 966-74

Dempsey J F, Low D A, Kirov A S, and Williamson J F 1999 Quantitative optical densitometry using scanning film digitizers *Med.Phys.* **26** 1721-1731

Devic S, Kirov A S, Dempsey J F, and Williamson J F 1999 A robust algorithm for Spikes Elimination from 2D CCD Low-level Light output Measurements in the Presence of Ionizing Radiation Field (abstract) *Med. Phys.* **26** 1161

Devic S, Seuntjens J, Hegyi G, Podgorsak E B, Soares C G, Kirov A S, Ali I, Williamson J F, and Elizondo A 2004 Dosimetric Properties of Improved GafChromic Films for Seven Different Digitizers *Med. Phys.* **31** 2392-2401

Duggan L, Hood C, Warren-Forward H, Haque M, and Kron T 2004 Variations in dose response with x-ray energy of LiF:Mg,Cu,P thermoluminescence dosimeters: implications for clinical dosimetry *Phys. Med. Biol.* **49** 3831-3845

Flühs D, Heintz M, Indenkämper F, Wiczorek C, Kolanoski H, and Quast U 1996 Direct reading measurement of absorbed dose with plastics scintillators - the general concept and applications to ophthalmic plaque dosimetry *Med. Phys.* **23** 427-34

Flühs D, Anastassiou G, Wening J, Sauerwein W, and Bornfeld N 2004 The design and the dosimetry of bi-nuclide radioactive ophthalmic applicators *Med Phys.* **31** 1481-8

Gustavsson H, Bäck S Å J, Medin J, Grusell E, and Olsson L E 2004 Linear energy transfer dependence of a normoxic polymer gel dosimeter investigated using proton beam absorbed dose measurements *Phys. Med. Biol.* **49** 3847-3855

Horrocks D L 1964 Pulse height energy relationship of a liquid scintillator for electrons of energy less than 100 keV *Nucl. Instr. Meth.* **30** 157-160

Hungerford J L 2003 Current trends in the treatment of ocular melanoma by radiotherapy *Clin. Experiment Ophthalmol.* **31** 8-13

Kaulich T W, Zurheide J, Haug T, Budach W, Nusslin F, and Bamberg M 2004 On the actual state of industrial quality assurance procedures with regard to (106)Ru ophthalmic plaques *Strahlenther Onkol.* **180** 358-64

Kirov A S, Meigooni A S, Zhu Y, and Williamson J F 1995 TLD, Diode and Monte Carlo Dosimetry of Ir-192 Source for High Dose-Rate Brachytherapy *Phys. Med. Biol.* **40** 2015-2036

Kirov A S, Hurlbut C, Dempsey J F, Shrinivas S B, Epstein J W, Binns W R, Dowkontt P F, and Williamson J F 1999a Towards two dimensional brachytherapy dosimetry using plastic scintillator: New highly efficient water equivalent plastic scintillator materials *Med. Phys.* **26** 1515-1523

Kirov A S, Piao Z, Devic S, Miller T, Binns W, and Epstein J 1999b Tests of a new three dimensional dosimetry method using liquid scintillator (abstract) *Med. Phys.* **26** 1069-1070

Kirov A S, Binns W R, Dempsey J F, Epstein J W, Dowkontt P F, Shrinivas S, Hurlbut C, and Williamson J. F 2000a Towards two dimensional brachytherapy dosimetry using plastic scintillator: Localization of the scintillation process *Nucl. Instr. Meth.* **A439** 178-188

Kirov A S, Piao Z, Devic S, Shrinivas S, Beddar A S, Binns W R, Kinsella T K, and Sibata C H 2000b An Estimate of the Perturbing Effect of Cerenkov Radiation to the Signal from a Liquid Scintillator Volume Irradiated by a Megavoltage Photon Beam (on a Compact Disc) *Proc. World Congress on Medical Physics and Biomedical Engineering and Proceedings of the 22nd Annual International Conference of the IEEE Engineering in Medicine and Biology Society p.4 pages paper (Chicago, July 23-28,2000)*

Kirov A S, Shrinivas S, Hurlbut C, Dempsey J F, Binns W R, and Poblete J L 2000c New water equivalent liquid scintillator solutions for 3D dosimetry *Med. Phys.* **27** 1156-1164

Kirov A S 2001 Towards Three Dimensional Scintillation Dosimetry using Tomographic Reconstruction *Proc. Book of Abstracts, Frontier Science Research Conferences, Radiation Oncology Physics-2001 p.29-33 (San Diego, CA, Feb. 2001)*

Kirov A S, Paio Z, Winkler M, Xue J, Devic S, Binns W R, Kusner M, Hurlbut C, Kinsella T, and Sibata C 2002a Measurement of scintillation light attenuation in liquid scintillation solutions for 3D dosimetry (abstract) *Med. Phys.* **29** 1208

Kirov A S, Paio Z, Winkler M, Devic S, Miller T R, Binns W R, and Epstein J 2002b 3D Dose Measurement and Imaging Method based on Optical Emission Tomography of Scintillation Solutions *Proc. Second European Medical and Biological Engineering Conference, IFMBE Proceedings, Vol.3, Part 2, p.1108-1109 (Vienna, Austria, Dec. 4-8, 2002,)*

Maryański M J, Zastavker Y Z, and Gore J C 1996 Radiation dose distributions in three dimensions from tomographic optical density scanning of polymer gels : II. Optical properties of the BANG polymer gel *Phys. Med. Biol.* **41** 2705-2717

Niroomand-Rad A, Chiu-Tsao S-T, Soares C G, Meigooni A S, and Kirov A S 2005 Comparison of Uniformity of Dose Response of Double Layer Radiochromic Films (MD-55-2) Measured at 5 Institutions *Physica Medica* **In Press**

Olsson L E, Bäck S Å J, Magnusson P, and Harraldsson P 1998 "3D Dosimetry using Gels and MRI" in "Imaging in radiation therapy", (Madison, WI: Medical Physics Publishing)

Onori S, De Angelis C, Fattibene P, Pacilio M, Petetti E, Azario L, Miceli R, Piermattei A, Tonghi LB, Cuttone G, and Lo Nigro S 2000 Dosimetric characterization of silicon and diamond detectors in low-energy proton beams. *Phys Med Biol.* **45** 3045-58

Palm Å, Kirov A S, and LoSasso T 2004 Predicting energy response of radiographic film in a 6 MV x-ray beam using Monte Carlo calculated fluence spectra and absorbed dose *Med. Phys.* **31** 3168-78

Perera H, Williamson J F, Monthofer S P, Binns W R, Klarmann J, Fuller G L, and Wong J W 1992 Rapid two-dimensional dose measurement in brachytherapy using plastic scintillator sheet: Linearity, signal to noise ratio, and energy response characteristics *Int. J. Rad. Onc. Biol. Phys.* **23** 1059-1069

Peron M N and Cassette P 1996 A Compton Coincidence Study of Liquid Scintillator response in the 1-20 keV energy range *Nucl. Instr. & Meth., A* **369**, 344-7

Piao Z and Kirov A S 2001 Effect of Median Root Prior (MRP) regularization on the accuracy and convergence of maximum likelihood expectation maximization algorithm applied to 3D scintillation dosimetry (abstract on the AAPM web-site) *Proc. 2001 Annual Meeting of the American Association of Physicists in Medicine (Salt Lake City, UT, July 2001)*

Seuntjens J P, Ross C K, Shortt K R, and Rogers D W O 2000 Absorbed-dose beam quality conversion factors for cylindrical chambers in high-energy photon beams *Med. Phys.* **27** 2763-2779

Snyder D L, Miller M I, Thomas L I Jr, and Politte D G 1987 Noise and edge artifacts in maximum-likelihood reconstructions for emission tomography *IEEE Trans. Med. Imaging* **MI-6** 228-238

Soares C G, Vynckier S, Jaervinen H, Cross W G, Sipila P, Fluhs D, Schaeken B, Mourtada F A, Bass G A, and Williams T T 2001 Dosimetry of beta-ray ophthalmic applicators: comparison of different measurement methods *Med. Phys.* **28** 1373-1384

Trichter S, Amols H, Cohen G N, Lewis D, LoSasso T, and Zaider M 2002 Accurate dosimetry of Ru-106 ophthalmic applicators using GafChromic film in a solid water phantom (abstract) *Med. Phys.* **29** 1349

Turian J, Smith B, Bernard D, and Chu J 2004 A Convolution Method for IMRT Verification Using the AS500 EPID *Med. Phys.* **31** 1821

Wallis J W and Miller T R 1993 Rapidly Converging Iterative Reconstruction Algorithms in Single-Photon Emission Computed Tomography *The Journal of Nuclear Medicine* **34** 1793-1800

Williamson J F, Dempsey J F, Kirov A S, Monroe J I, Binns W R, and Hedtjärn H 1999 Plastic scintillator response to low-energy photons *Phys. Med. Biol.* **44** 857-871

Figure Captions

Figure 1. A photograph (a) and a top view schematic (b) of the experimental arrangement.

Figure 2. Illustration of the attachment of the CCX plaque inside the liquid scintillator cell. View from the bottom showing also the white Teflon strip in the top plate used to seal the cell.

Figure 3. Average single projection image frame, background and spike corrected, and after smoothing and binning as described in Section 2.4. Sixty four similar frames obtained under different angles were passed to the MLEM algorithm to reconstruct the scintillation light emission density.

Figure 4. Relative depth dose profiles as a function of the distance from the inner surface of a CCX eye plaque, as measured by radiochromic film (RCF) and a diode (symbols) and the 3DSD method (curves). In its current implementation the 3DSD method does not account for the opaqueness of the plaque, which results in unrealistically low relative dose within 5 mm from the plaque surface.

Figure 5. A comparison of 3DSD measured relative dose-rate contours (in cGy/h) in slices at (a) 4.5 mm, (b) 5.4 mm, (c) 6.4 mm, and (d) 7.4 mm from the inner surface of the plaque, to the result from the MSKCC radiochromic film (RCF) measurement (thick solid lines). The 3DSD data (dotted and dashed lines) were normalized to the absolute RCF measurements at the peak. The dotted lines correspond to the relative emission density and the dashed lines to the relative dose deduced from the emission density after corrections and liquid scintillator point spread function deconvolution.

Figure 6. A relative comparison of dose-rate profiles obtained with the 3DSD method to radiochromic film (RCF) and diode profiles through the center of the slices shown in Figure 5 at (a) 4.5 mm, (b) 5.4 mm, (c) 6.4 mm, and (d) 7.4 mm from the inner surface of the plaque (a-d) and to diode profiles at 8.5 and 10 mm distances (e-f). Vertical profiles are shown on the left and horizontal on the right. The 3DSD and diode profiles are normalized to the absolute RCF measurements at the highest point in each slice a-d as in Figure 5. For the profiles at 8.5 and 10 mm (e-f) the 3DSD profiles are scaled with the normalization factor from the slice at 7.4 mm and the diode profiles are normalized at the highest point of the deduced relative dose-rate.

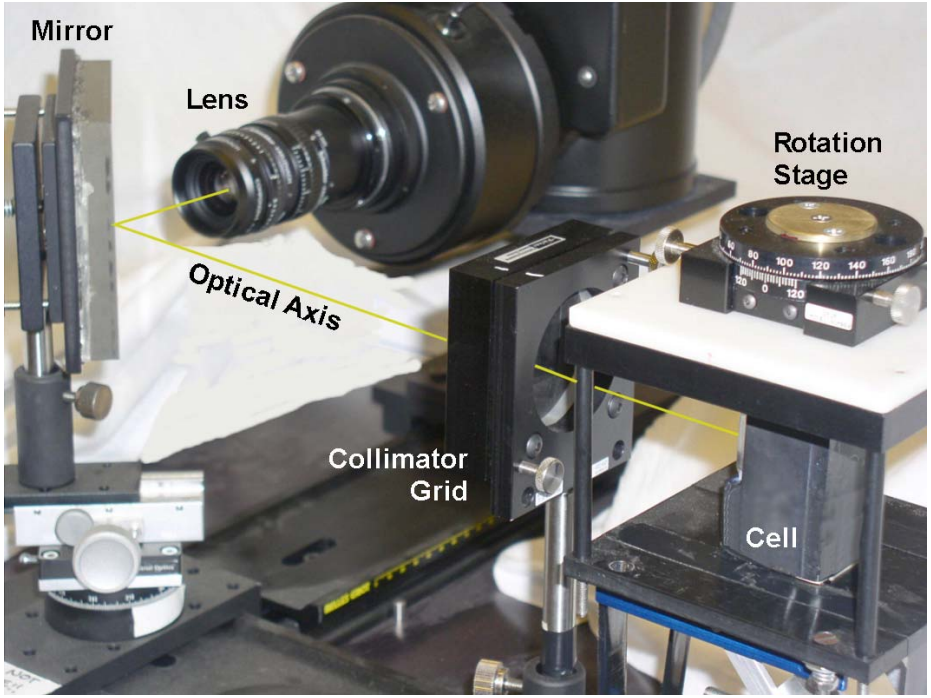


Fig.1.a.

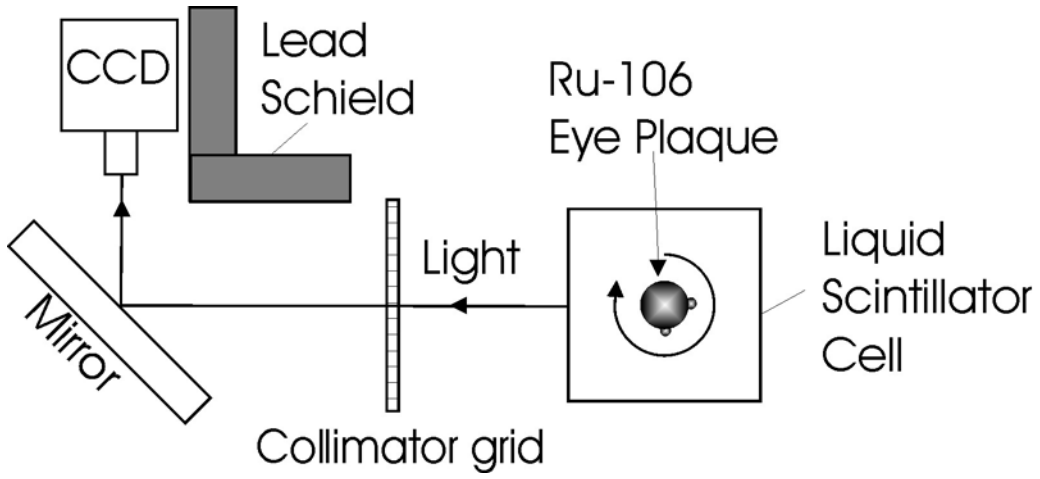


Fig.1.b.

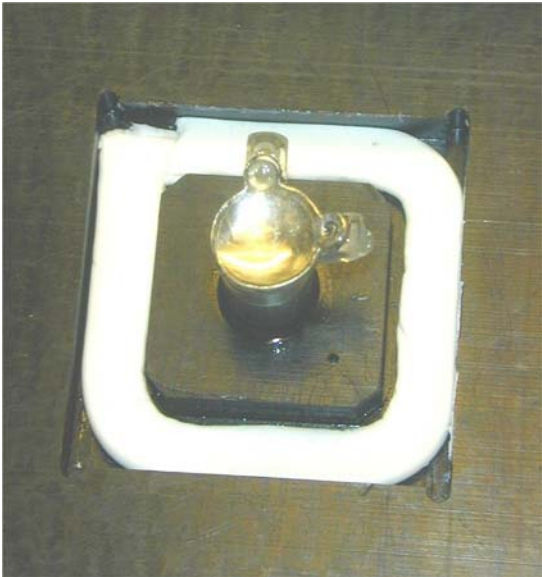


Fig.2.

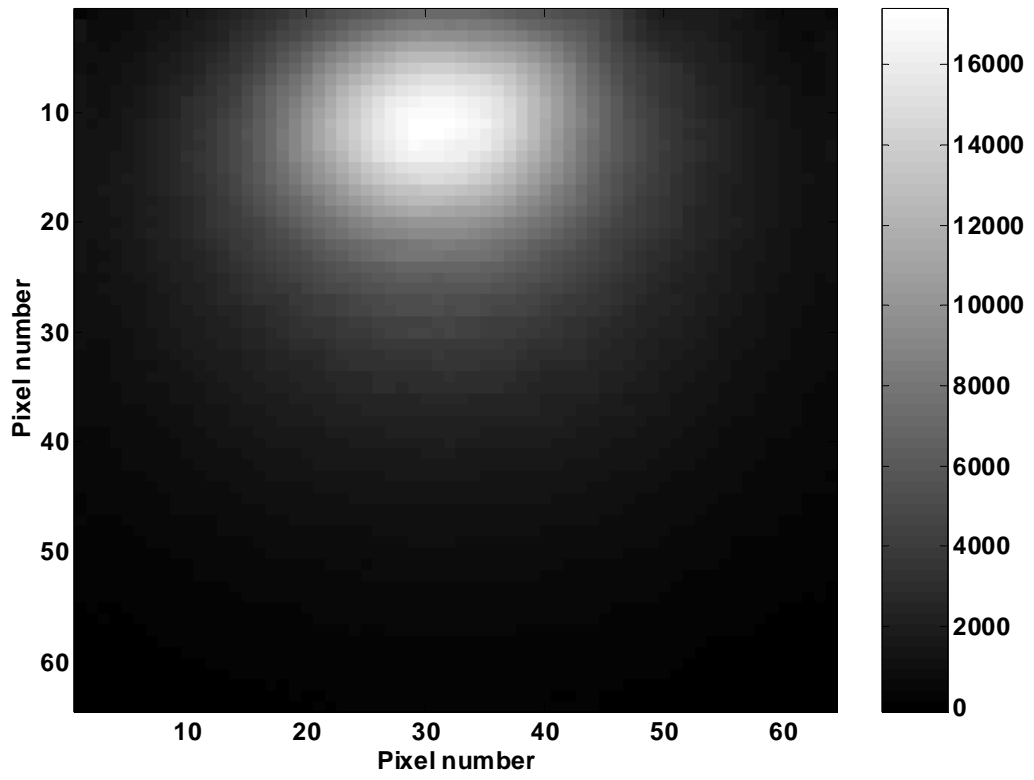


Fig.3.

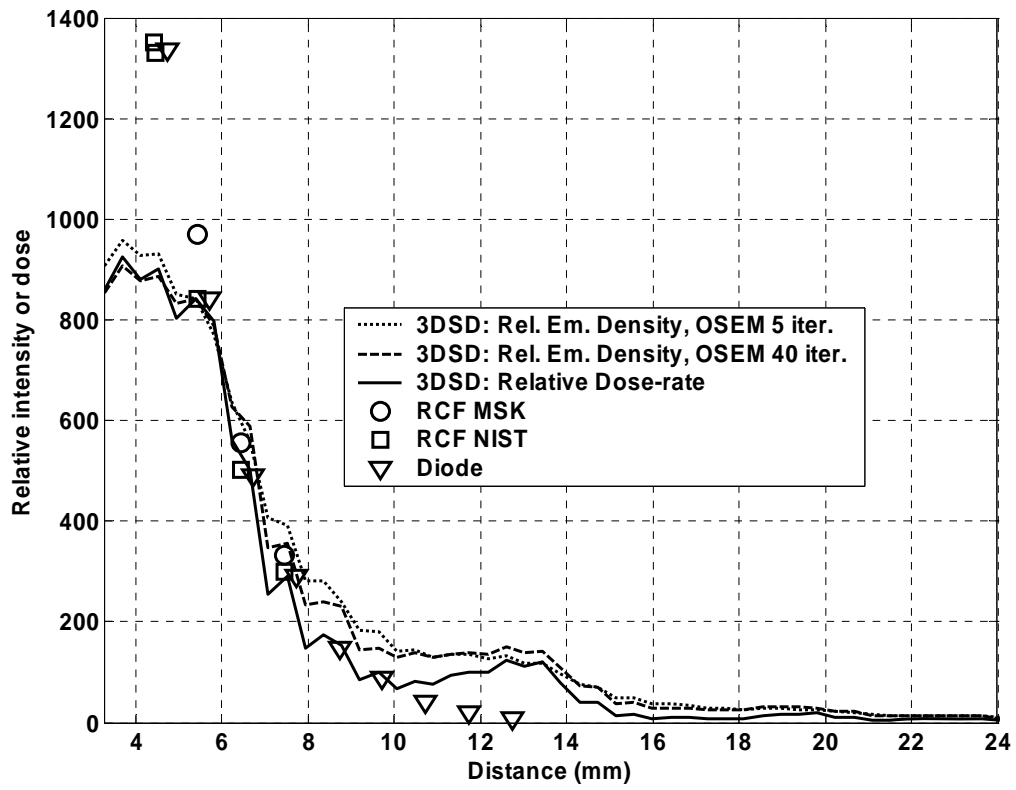
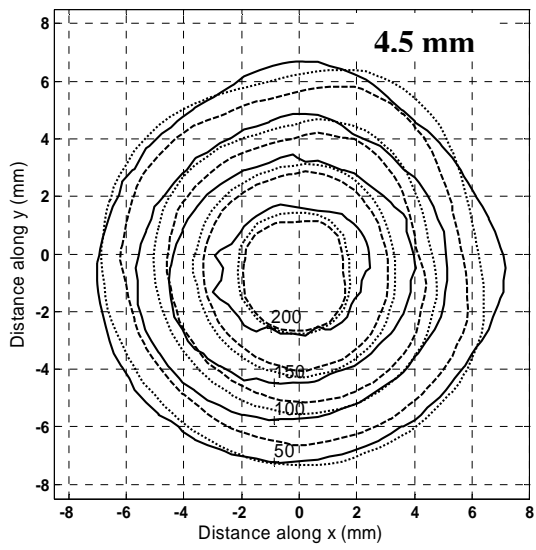
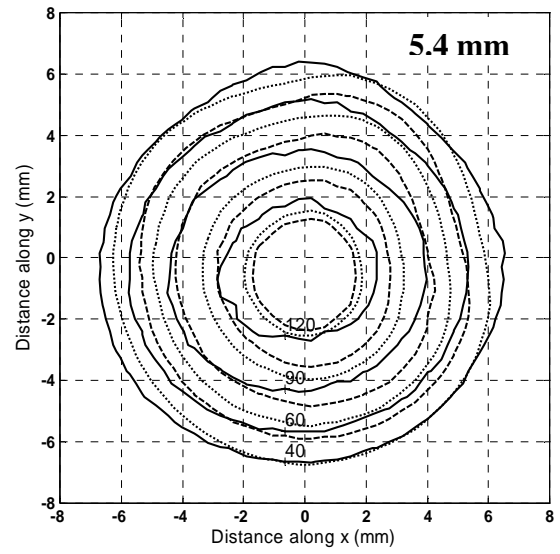


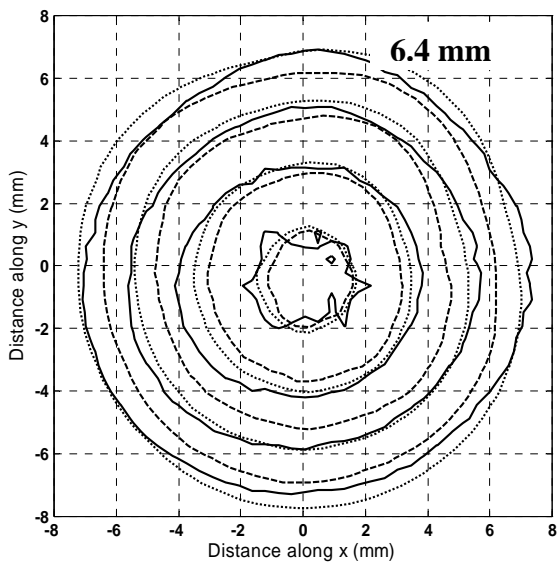
Fig.4.



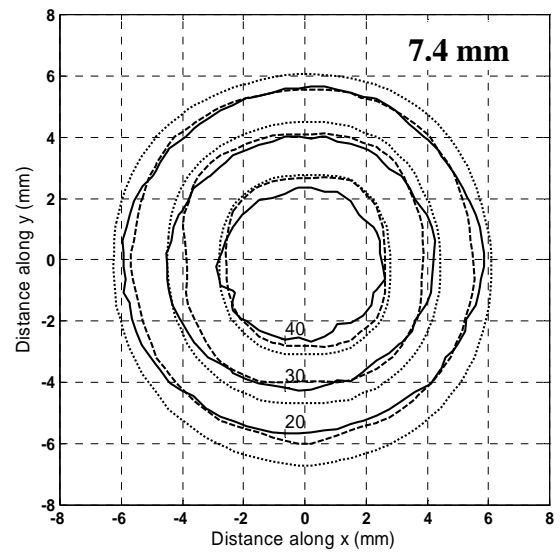
(a)



(b)

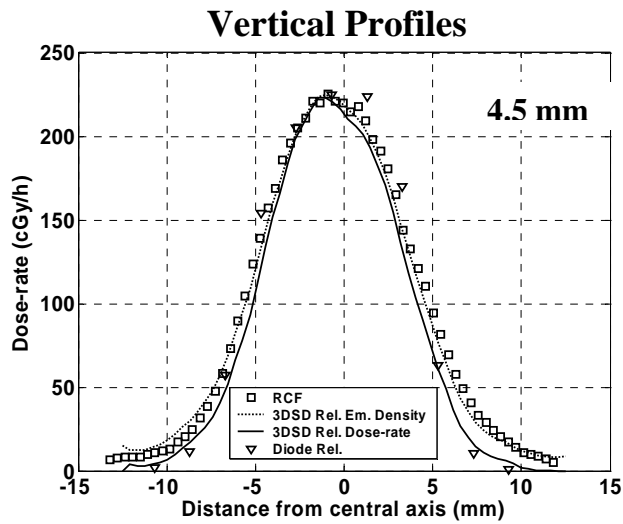


(c)

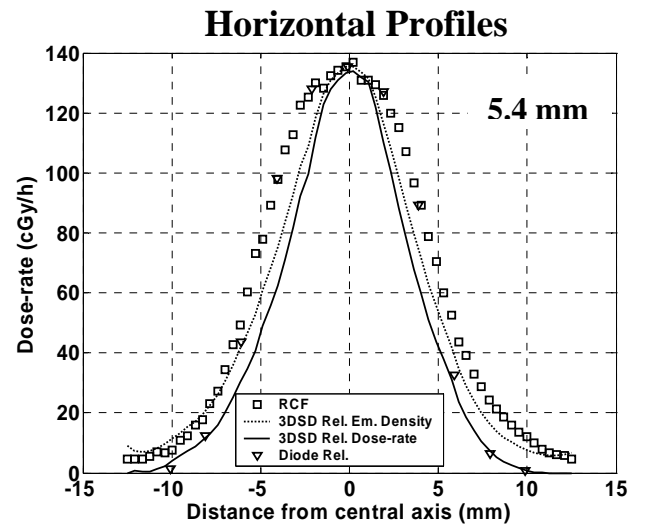


(d)

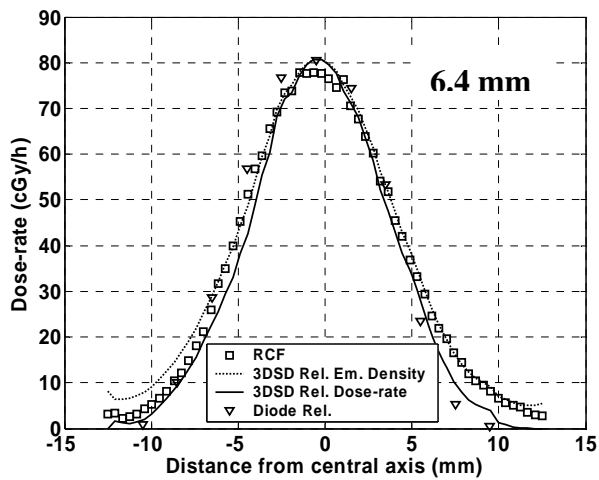
Fig. 5.



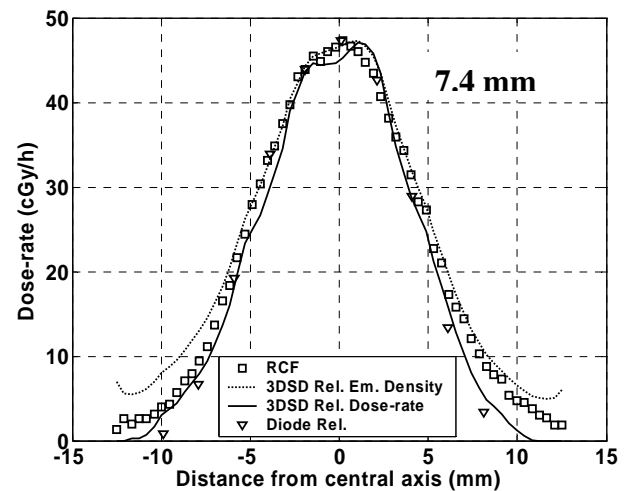
(a)



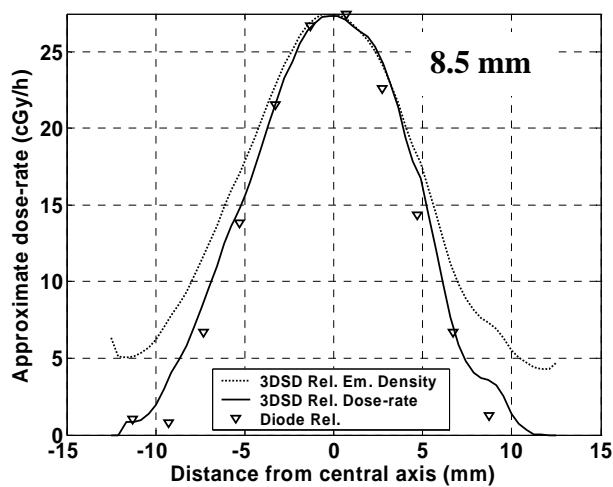
(b)



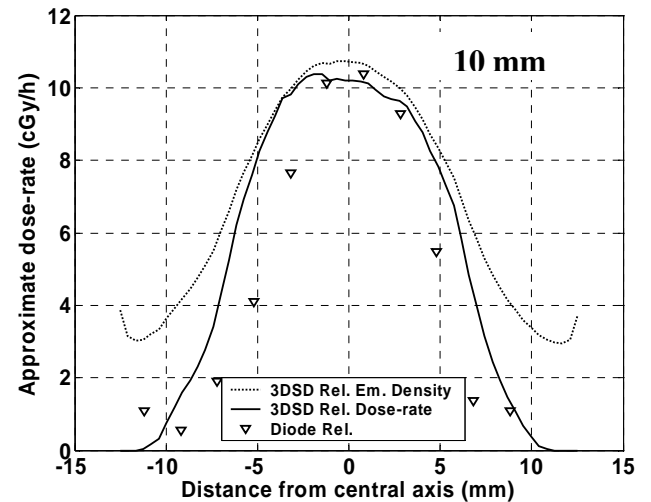
(c)



(d)



(e)



(f)

Fig. 6